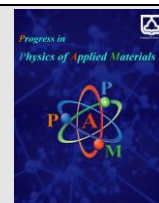




Semnan University



# Simulation of size effects on the optical properties of KTP nanoparticles

Nematollah Abdi Valikchali, Majid Jafar Tafreshi, Fatemeh Shariatmadar Tehrani\*

Faculty of Physics, Semnan University, P.O.Box 35195-363, Semnan, Iran.

## ARTICLE INFO

### Article history:

Received: 2 May 2024

Revised: 3 July 2024

Accepted: 9 July 2024

### Keywords:

KTP nanoparticles

Optical properties

Particle size

COMSOL Multiphysics

Band gap

Refractive index

## ABSTRACT

KTiOPO<sub>4</sub> (KTP) is a non-linear optical crystal with high non-linear optical coefficients and an optical damage threshold that has wide applications in optical devices. The optical properties of KTP nanoparticles are critical in nanotechnology. This study employs COMSOL Multiphysics software and the finite element method (FEM) in order to examine the effects of particle size (10 to 100 nm) on the optical properties of spherical KTP nanoparticles, including refractive index dispersion, scattering cross-section, band gap energy, and cut-off wavelength. The obtained results were compared with the available experimental data. The results of this research showed that the refractive index dispersion and scattering cross-section for KTP nanoparticles follow the FEM model and Mei's theory for spherical nanoparticles. For radiated light with a specific wavelength, decrease in the size of KTP nanoparticles causes a decrease in the scattering cross-section, refractive index, and absorption edge wavelength. By decreasing the particle size from 100 nm to 50 nm, the refractive index remained almost constant at 1.81 and decreased slightly with further decrease in particle size to 20 nm. Also, reducing the particle size below 20 nm decreased the refractive index to 1.80. The band gap energy of KTP nanoparticles increased from 3.9 eV to 6.27 eV as the particle size decreased from 100 nm to 10 nm. However, a significant increase in band gap energy was observed when particle size decreased from 20 nm to 10 nm. The results of the simulation work were found to be consistent with the previous reports.

## 1. Introduction

The chemical formula for potassium titanyl phosphate, or KTP, is KTiOPO<sub>4</sub>, and it has gained popularity in recent years due to its excellent nonlinear optical applications, especially for doubling the frequency of 1064 nm radiation from Nd:YAG lasers [1-4]. In 1976, Zumsteg et al. identified KTP as a nonlinear optical (NLO) material [5]. It crystallizes in the non-symmetric Pna21 space group in an orthorhombic system [6]. It is one of the most widely utilized ferroelectric materials in the field of electro-optic and nonlinear optics applications [7, 8]. Bulk KTP single crystal has biaxial optical properties and is chemically inert. It exhibits outstanding features including wide acceptance angles, high optical damage threshold, high nonlinear-optical coefficients, and thermally stable phase matching [9-

13]. Table 1 lists the key characteristics of bulk KTP crystal [5].

Generally, researchers refer to crystalline solids with grain sizes smaller than 100 nm as nanocrystalline materials [14]. Because of surface effects, size, and quantum confinement, they behave mechanically, electrically, physically, and chemically different compared to their bulk counterpart.

When a substance's size is reduced to the nanoscale, its physical properties undergo modifications and enhancements. These characteristics are shape- and size-independent at the macroscopic level, but when a material is shrunk to the nanoscale, significant changes are observed in the physical parameters [15-23]. Specifically, decreasing the size of particles to nanoscale induces appreciable

\* Corresponding author.

E-mail address: [f\\_tehrani@semnan.ac.ir](mailto:f_tehrani@semnan.ac.ir)

### Cite this article as:

Abdi Valikchali, N., Jafar Tafreshi, M. and Shariatmadar Tehrani, F., 2024. Simulation of size effects on the optical properties of KTP nanoparticles.

*Progress in Physics of Applied Materials*, 4(2), pp.123-133. DOI: [10.22075/PPAM.2024.33978.1098](https://doi.org/10.22075/PPAM.2024.33978.1098)

© 2024 The Author(s). Journal of Progress in Physics of Applied Materials published by Semnan University Press. This is an open access article under the CC-BY 4.0 license. (<https://creativecommons.org/licenses/by/4.0/>)

changes in optical and electronic properties of materials such as band gap energy, absorbance, refractive index, dielectric constant, and electrical capability compared to its bulk form [24]. For the past few decades, researchers have theoretically studied the physical characteristics of materials, including band gap energy, melting temperature, dielectric constant, and electrical susceptibility. These quantities are crucial for the creation of optical and electronic nano-devices.

According to theoretical studies, cohesive energy decreases as nanomaterials such as Si, Sn, Pb, and Bi get smaller in size because there are more dangling bonds, which lower the melting temperature and increase the band gap energy [15]. Also, reducing the size of the nanoparticle reduces its refractive index, as reported by the previous studies. The effects of size on the refractive index of nanoparticles including Si, ZnO, CdS, InP, TiO<sub>2</sub>, and Ge have been theoretically studied in the literature [15-17]. In addition, theoretical studies have been reported about the effects of particle size on the optical properties and band gap of nanoparticles and nanostructures such as Si, ZnO, CdS, InAs, GaN, and InP [15, 20].

Several reported works are available about the synthesis of KTP nanoparticles and nanostructures by different methods such as Pechini, sol-gel, mechanical-chemical, combustion, and co-deposition, and the experimental measurement of their physical and optical properties (linear and nonlinear) [25-34] and applications such as nanofilters and nanomembranes [25-34]. Thuy et al., for example, used a simulation model with the Finite-Difference Time-Domain (FDTD) method and a direct laser writing technique to study the production of any photonic structure of polymer-based nonlinear KTP nanoparticles, both experimentally and theoretically [32]. They have studied the second-harmonic generation (SHG) of individual KTP nanoparticles with a size of around 100 nm under a pulsed laser excitation wavelength of 1064 nm. KTP NPs displayed a higher nonlinear coefficient than the bulk one, and the SHG was totally stable at ambient temperature. The signal-to-noise ratio was high because of its transparency at both fundamental and SH wavelengths. Additionally, they showed off a superb method for generating desired polymeric photonic structures with a single KTP nanoparticle [32]. Furthermore, Zhou et al. have studied KTP nanocrystals using atomic force microscopy (AFM) and second-harmonic generation microscopy (SHGM) [33]. Nikolaev et al. have studied how cluster ion characteristics affect the development of nanostructures on the KTP surface [34].

Despite several experimental studies on the synthesis of KTP nanoparticles and the investigation of their properties and applications, there are only a few reports about the effects of particle size on the optical properties of KTP nanostructures. Furthermore, there is a lack of extensive reporting on the use of computer simulation to explore and enhance the optical properties of these nanostructures. To the best of the authors knowledge, no theoretical research has yet been done using computer modeling to examine how the size of the KTP nanoparticle affects its optical characteristics, such as the scattering cross-section, refractive index, and band gap energy. Therefore, this work could open the way for further research to improve the

optical properties of KTP nanoparticles and their use in optical devices, with the advantage of saving time and costs in research. This study employed COMSOL Multiphysics software to simulate and analyze the effects of size on the optical properties of KTP spherical nanoparticles with a circular cross-section in two dimensions, using the finite element method (FEM). The outcomes were compared with those of other available works.

**Table 1.** Properties of KTP bulk crystal [5]

<b>Structural and Physical Properties</b>	Chemical formula: KTiOPO <sub>4</sub> (KTP)			
	Crystal structure: Orthorhombic			
	space group: Pna21			
	point group mm2			
	Cell parameters: a=6.404 Å, b=10.616 Å, c=12.814 Å, Z=8,			
	Melting point: 1172° C			
	Curie point: 936° C,			
	Mohs hardness: ≈5,			
	Density: 3.01 g/cm <sup>3</sup> ,			
	Color: colorless,			
<b>Optical Properties</b>	Hygroscopic susceptibility: no,			
	Specific heat: 0.1643 cal/g°C,			
	Thermal conductivity: 0.13 W/cm/K,			
	Electrical conductivity: 3.5*10 <sup>-8</sup> s/cm			
	(c-axis, 22° C, 1kHz)			
	Transmitting range: 350 nm – 4500 nm			
	Refractive indices:			
		nx	ny	nz
	1064 nm:	1.7377	1.7453	1.8297
	532 nm:	1.7780	1.7886	1.8887
Absorption: α < 1% cm <sup>-1</sup> @ 1064nm and 532nm				

## 2. Modelling and simulation

Using the commercial finite element analysis software COMSOL Multiphysics package, this study models spherical KTP nanoparticles with varying particle sizes (10–100 nm) and simulates their optical (linear) properties, including refractive index dispersion, scattering cross section, band gap energy, and cut-off wavelength.

### 2.1. Theoretical Framework

The theoretical framework of this study is the theory of light absorption, known as Mei theory, that was introduced in 1908 [35-40]. It illustrates how incident electromagnetic waves cause coherent oscillations of electrons, which polarize the nanoparticles, and is based on Maxwell's equations, utilizing ideas from classical electrodynamics theory. The Mie theory describes how electromagnetic light scatters when a spherical particle is submerged in a continuous environment using mathematical and physical principles [10, 15]. The Helmholtz equation can be used to illustrate the electric field (E) and magnetic field (H), two components of the electromagnetic radiation field. Accordingly, the scattering amplitude functions in terms of the extinction and scattering coefficients are obtained using the series of E and H. For a spherical particle of radius

R, the extinction cross-section and the scattering cross-section are provided as follows using Mie theory [38]:

$$\sigma_{ext} = \frac{2}{x^2} \sum_{n=1}^{\infty} (2n + 1) [Re(a_n + b_n)] \quad (1)$$

$$\sigma_{sca} = \frac{2}{x^2} \sum_{n=1}^{\infty} (2n + 1) (|a_n|^2 + |b_n|^2) \quad (2)$$

$$\sigma_{sca} = \sigma_{ext} - \sigma_{abs} \quad (3)$$

where  $\sigma_{abs}$  is the absorption cross-section and  $x$  is the size parameter given by the following relation:

$$x = \frac{2\pi R \epsilon_m}{\lambda} \quad (4)$$

where  $\lambda$  is the wavelength of the incident light,  $R$  is the particle's radius, and  $\epsilon_m$  is the dielectric constant of medium. The Mie scattering coefficients in terms of the Riccati-Bessel equations are  $a_n$  and  $b_n$  [38]:

$$a_n = \frac{m\psi_n(mx)\psi_n(x) - \psi_n(y)\psi_n(mx)}{m\psi_n(mx)\xi_n(x) - \xi_n(x)\psi_n(mx)} \quad (5)$$

$$b_n = \frac{\psi_n(mx)\psi_n(x) - m\psi_n(y)\psi_n(mx)}{\psi_n(mx)\xi_n(x) - m\xi_n(x)\psi_n(mx)} \quad (6)$$

in which  $\psi_n(x)$  and  $\xi_n(x)$  are Riccati-Bessel functions and  $m = \frac{\epsilon}{\epsilon_m}$ , where  $\epsilon$  is the complex dielectric constant of nanoparticle and  $\epsilon_m$  is the real dielectric constant of surrounding medium. The scattering approach leads to the expression for extinction cross section  $\sigma_{ext}$  as:

$$\sigma_{ext} = \frac{24\pi^2 R^3 \epsilon_m^{2/3}}{\lambda} \frac{\epsilon_2}{(\epsilon_1 + 2\epsilon_m)^2 + \epsilon_2^2} \quad (7)$$

where  $\epsilon_1$  and  $\epsilon_2$  are the real and imaginary components of the dielectric constants, respectively.

The dispersion relation of refractive index can be expressed by Sellmeier's equations [10, 41]. These equations for KTP bulk crystal are expressed as follows:

$$\begin{aligned} \eta_x^2 &= 9.54967 + \frac{1.14398\lambda^2}{\lambda^2 - 13637} \\ \eta_y^2 &= 9.72515 + \frac{1.26864\lambda^2}{\lambda^2 - 13889} \\ \eta_z^2 &= 13.4416 + \frac{2.29045\lambda^2}{\lambda^2 - 11799} \end{aligned} \quad (8)$$

where  $\eta_x$ ,  $\eta_y$ , and  $\eta_z$  are the components of refractive index and  $\lambda$  is the wavelength of the radiation.

In the nanoscale, due to the increase in the surface to volume ratio and the quantum confinement effect, the optical properties of materials are controlled significantly by their particle size and shape. To investigate the effects of particle size on the refractive index and dielectric constant of KTP nanoparticles, first the equation related to the refractive index of the bulk material is considered based on its characteristics and then the equations related to the nanoparticles are extracted as follows [16, 17]:

$$\eta - 1 = \frac{Nq_e^2}{2\epsilon_0 m \omega_0^2} \quad (9)$$

$$\frac{n_D}{n} = \left(1 - \frac{N_s}{2n}\right) \quad (10)$$

$$\eta_{D,\alpha} = 1 + (\eta - 1) \left(1 - \frac{\beta\alpha}{D}\right) \left(1 - \frac{N_s}{2n}\right) \quad (11)$$

$$\epsilon_{D,\alpha} = (\eta_{D,\alpha})^2 \quad (12)$$

where  $\eta$  is refractive index for the bulk material,  $\eta_{D,\alpha}$  is refractive index for nanoparticles,  $N$  is the number of atoms per unit volume,  $\omega_0$  is the natural angular frequency of electrons in atoms of the bulk material,  $m$  is the electron mass,  $q_e$  is the electron charge,  $\alpha$  is the shape factor,  $n_D$  and  $n$  are the number of atoms inside the volume of nanomaterial and bulk material respectively,  $N_s$  is the number of surface atoms for the nanomaterial. Also,  $d$  is the diameter of the atom,  $D$  is the diameter of the nanoparticle,  $\beta$  is a material dependent constant, and  $\epsilon_{D,\alpha}$  is the dielectric constant of nanoparticles.

The theory related to the optics of a bulk sample with direct transition, with the assumption of irradiating light with energy of  $hf$  and intensity of  $I_0$  to a sample with thickness of  $t$ , band gap energy of  $E_g$ , and transmission intensity  $I$ , the absorption coefficient  $\alpha$ , and complex refractive index ( $\underline{\eta}$ ) are given as follows:

$$E_g (eV) = \frac{hc}{\lambda_{cut-off}} \quad (13)$$

$$\alpha = \frac{4\pi\kappa}{\lambda_0} \quad (14)$$

$$\underline{\eta} = \eta + i\kappa \quad (15)$$

$$I = I_0 e^{-\alpha t} \quad (16)$$

$$(\alpha hf)^n = B(hf - E_g) \quad (17)$$

where  $h$  is plank constant,  $f$  is frequency of radiation,  $c$  is speed of light,  $\lambda$  is cut-off wavelength,  $\lambda_0$  is vacuum wavelength,  $\eta$  is the real part of refractive index,  $\kappa$  is the imaginary part of refractive index.  $\kappa$  is called the optical extinction coefficient, and related to absorption coefficient.  $n$  in equation (17) is 2 for direct transition and  $\frac{1}{2}$  for indirect transition, and  $B$  is a constant parameter related to the structural properties of material.

The following equation has been introduced for the band gap energy of nanoparticles [18-23]:

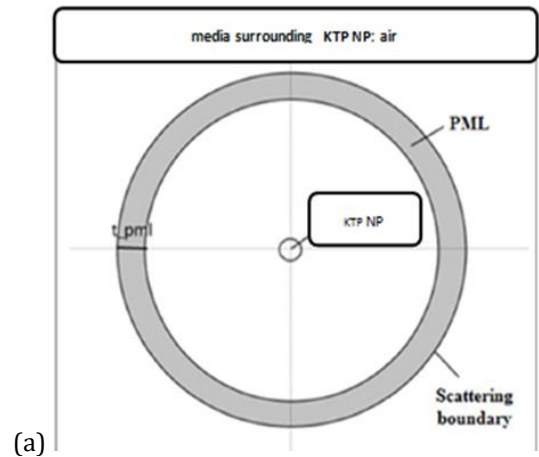
$$E_{gN} = E_{gB} \left(1 + \frac{3N_s}{4n}\right) = E_{gB} \left(1 + 3\alpha \frac{d}{D}\right) \quad (18)$$

where  $E_{gN}$  and  $E_{gB}$  indicate the band gap energy of nano and bulk materials, respectively.

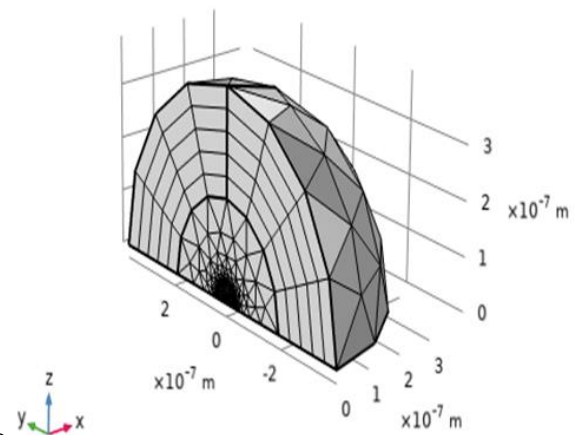
## 2.2. Simulation technique

The underlying partial differential equations are solved by the finite element method in the COMSOL Multiphysics software. It should be mentioned that the discretization of the modeling domains into smaller, more manageable domains called elements is how the finite element approach works. A set of equations covering all of the model's components is put together and solved to determine the solution. A spherical KTP particle with an air domain that has been shortened using a perfectly matched layer (PML) is regarded to be the simulation domain in order to calculate the refractive index dispersion based on Sellmeier equations with respect to the KTP particle size. The model resolves the Maxwell's equations for the electromagnetic radiation scattered by spherical KTP particles. Figure 1 displays the model geometry in which half of the system is simulated in order to preserve the symmetry of the system. The far-field calculations were carried out on the inner border of the PML. Using an incident plane wave flowing in the x direction and an electric field polarized along the z-axis, the simulation

computes the local electromagnetic field at each mesh point. Within the "Wave Optics" module, Electromagnetic Waves, Frequency Domain (EWFD) was the interface utilized in this simulation. The study was conducted in the frequency domain in three dimensions. Following the construction of the model and the application of materials to the relevant domains, the Perfectly Matched Layer (PML) and scattering boundary condition were defined, as seen schematically in Figure 2(a). After applying the mesh to the PML domain, the remaining structure was built in a free tetrahedral pattern, as seen in Figure 2(b). On the outside boundary of the PML, the scattering boundary condition was established. The Electromagnetic Waves, Frequency Domain (EWFD) interface adds the inclusion of "Wave Equation, Electric" physics. The refractive index dispersion of a specific KTP particle was obtained in this study using a parametric sweep, which was set for wavelengths between 400 and 1000 nm with a step size of 100 nm. A parametric sweep was established for particle size from 10 to 100 nm in steps of 10 nm to examine the effects of particle size on refractive index, band gap, cut-off wavelength, and scattering cross section. Moreover, in order to investigate the effects of particle size on band gap energy and absorption edge wavelength, in addition to the parametric solution for particles from 10 to 100 nm with a step of 10 nm, the experimentally reported results in the literature for KTP nanoparticles with the particle sizes of 54, 53.08, 47.58, 44.5, 39.42, 17.89, 17.47, 17.24, 17.19, 17.16, 17.06, 16.31, 15.90, 15.86, 15.71, 15.11, 14.95, 14.61, 14, 13.76, 13.64, 13.49, 12.90, 12.78, and 12 nm are also simulated for more exact comparison with the experimental data.



(a)



(b)

Fig. 2. (a) The model's schematic diagram, and (b) the simulation's 3D mesh structure.

Also, similar to the photonic crystal, we assumed the model in 2D to be consisted of KTP nanoparticles with circular cross-section placed equidistant from each other in a cubic structure [42-44]. Certain wavelengths of light cannot enter the crystal structure because of the space between the particles. A given frequency range of waves is reflected rather than traveling through the crystal, depending on the spacing between the particles [44]. The photonic band gap is the term for this range of frequencies. Since this model has a repeated pattern, it is possible to use periodic boundary conditions and thus, only one particle is required for this simulation. The model geometry and its mesh are shown in Figures 3(a) and (b), respectively. This analysis has two primary problems. First, KTP's refractive index depends on frequency; second, the wavevector needs to be ramped in order to conform to the band diagram. The two combined complexities make it challenging to solve without reformulating the issue, even though each of these problems may be addressed alone with the eigenvalue solver. Consequently, a stationary solver has been used to define a nonlinear eigenvalue problem with the eigenvalue as an unknown [38, 39]. The electric field is normalized in the eigenvalue equation such that the average field over the domain is unity. Using an updated refractive index to the computed eigenvalue, the nonlinear solver determines the right eigenvalue. Moreover, the wavevector,  $k$ , can be swept by the parametric solver. The wavevector of propagating wave is considered in the simulation as boundary conditions for Floquet periodicity. The periodic condition was defined on the outer boundary of the square cell sides.

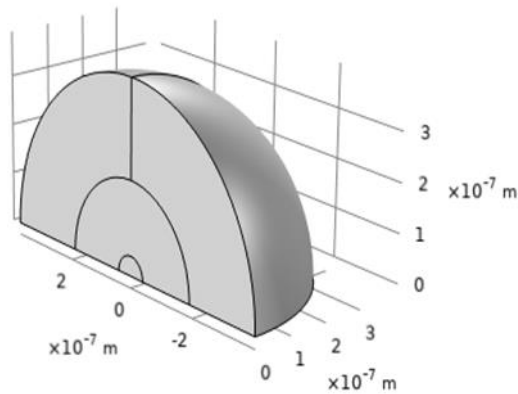


Fig. 1. The geometrical model used for simulation of optical properties of a KTP nanoparticle.

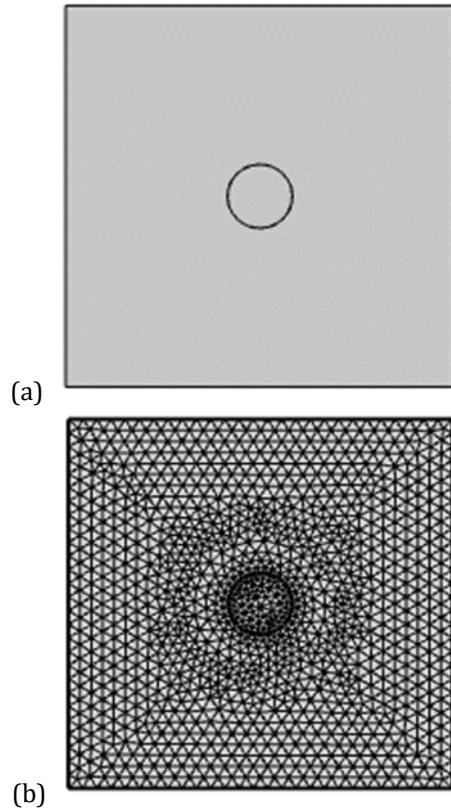


Fig. 3. (a) Geometry of the model, and (b) meshing construction of geometry.

### 3. Results and discussion

Considering a KTP spherical nanoparticle with a diameter of 10 nm exposed to radiation with wavelengths of 400-1000 nm with steps of 100 nm, the effect of the radiation wavelength on the scattering cross section is calculated. The obtained results, using equations 1, 2, 3, and 7, are shown in Table 2, which indicates gradual decreasing of scattering cross section with increasing radiation wavelength. Also, light with a wavelength of 400 nm was irradiated on nanoparticles with sizes of 10-100 nm with steps of 10 nm to show the effects of the size of nanoparticles on the scattering cross section. The obtained results are reported in Table 3, where the simulation results show that the scattering cross section increases with increasing the size of the KTP nanoparticles and the data are fitted to an exponential function with the equation:  $y=y_0+Ae^{R_0x}$  as plotted in Figure 4.

Table 2. Simulation results for the scattering cross section for a KTP nanoparticle with the diameter of 10 nm irradiated with different light wavelengths.

$\lambda$ (nm)	$\sigma_{\text{Sca}}$ (m <sup>2</sup> )
400	$43.896 \times 10^{-21}$
500	$16.816 \times 10^{-21}$
600	$84.862 \times 10^{-22}$
700	$41.804 \times 10^{-22}$
800	$22.734 \times 10^{-22}$
900	$13.939 \times 10^{-22}$
1000	$99.044 \times 10^{-23}$

Table 3. Simulation results for the scattering cross section of KTP nanoparticles with different sizes.

Size (nm)	$\sigma_{\text{Sca}}$ (m <sup>2</sup> )
10	$43.896 \times 10^{-21}$
20	$23.889 \times 10^{-19}$
30	$22.201 \times 10^{-18}$
40	$92.362 \times 10^{-18}$
50	$23.673 \times 10^{-17}$
60	$48.626 \times 10^{-17}$
70	$12.757 \times 10^{-16}$
80	$49.921 \times 10^{-16}$
90	$18.938 \times 10^{-15}$
100	$45.222 \times 10^{-15}$

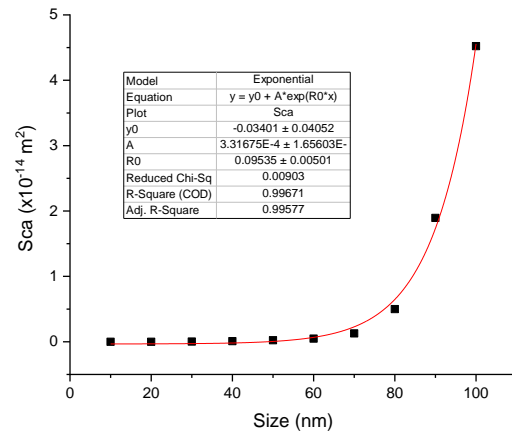


Fig. 4. Calculated variation of scattering cross section with size of KTP nanoparticles. The red curve is the fitted function to the calculated results.

According to Sellmeier equations (Eq. 8), the variation of refractive index at x direction ( $n_x$ ) and with the help of equations 14 and 15, absorption coefficient ( $\alpha_x$ ) as a function of wavelength (400-1000 nm) for a KTP nanoparticle (size: 20 nm) are plotted and shown in Figures 5, and 6 along with the experimental data obtained for a KTP crystal [10] for comparison. Relatively similar decreasing trends of refractive index with wavelength are observed for both sets of simulated and experimental data. These comparisons show that the refractive index and absorption coefficient of KTP in nanoscale are slightly lower than those of the bulk. In addition, the dependence of  $n$  components and absorption coefficient components on the KTP particle size are investigated by selecting the particle size in the range of 10 nm to 100 nm by the steps of 10 nm. For these purposes, the KTP particles are considered under light radiation with a wavelength of 400 nm. The simulated results for refractive index components, based on equations (9) to (11) are obtained and shown in Figure 7. According to this figure, by reducing the size from 100 nm to 50 nm, the refractive index remains constant at the values of 1.826, 1.838, and 1.893 respectively for  $n_x$ ,  $n_y$ ,  $n_z$  and decreases slightly with further decrease in particle size to 20 nm. However, by decreasing the particle size to the values below 20 nm, the refractive index decreases to 1.815, 1.827, and 1.840 respectively for  $n_x$ ,  $n_y$ ,  $n_z$ . These

results have shown that reducing the particle size in the nanoscale has a negligible effect on the refractive index, and its value lies slightly lower compared to the bulk counterpart. Also, the variations of x component of absorption coefficient of KTP spherical nanoparticles as a function of particle size are calculated according to equations 14 and 15, and shown in Figure 8. It should be noted that the particle size dependence of refractive index and absorption coefficient follow the similar trends. The calculated values of other components of absorption coefficient are listed in Table 4 which show the same trend as  $\alpha_x$ . Experimental data were not available to make a comparison in this part.

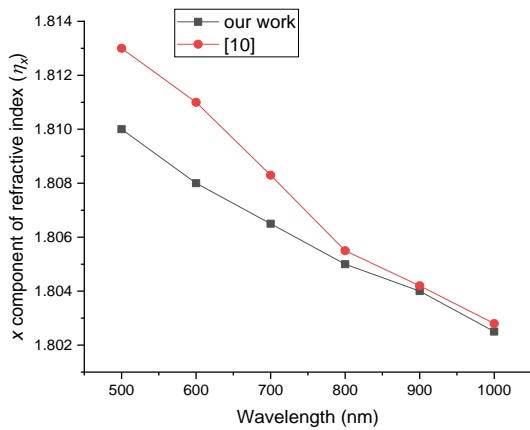


Fig. 5. The x component of refractive index dispersion for a simulated KTP spherical nanoparticle with the diameter of 20 nm (our work) and comparison to experimental data for KTP crystal from reference [10].

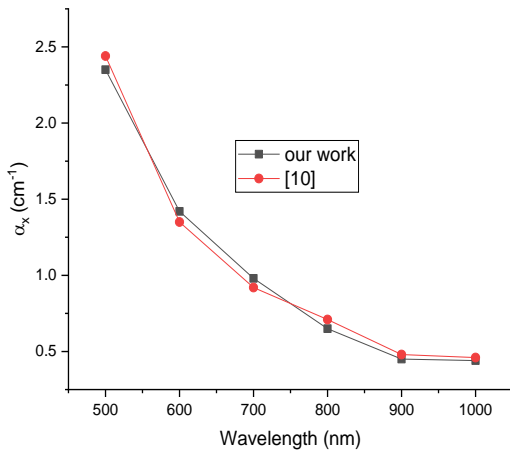


Fig. 6. The x component of absorption coefficient dispersion for a simulated KTP spherical nanoparticle with the diameter of 20 nm (our work) and comparison to the experimental data for KTP crystal from reference [10].

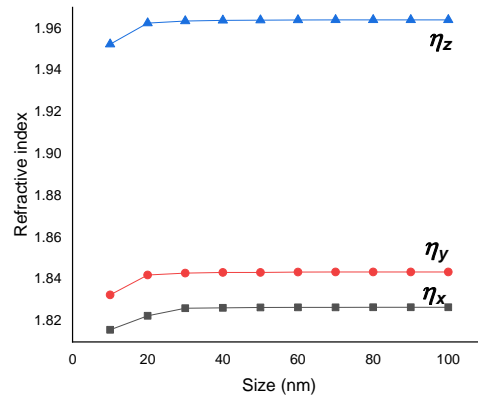


Fig. 7. The calculated components of refractive index ( $n$ ) for simulated KTP spherical nanoparticles with different diameters.

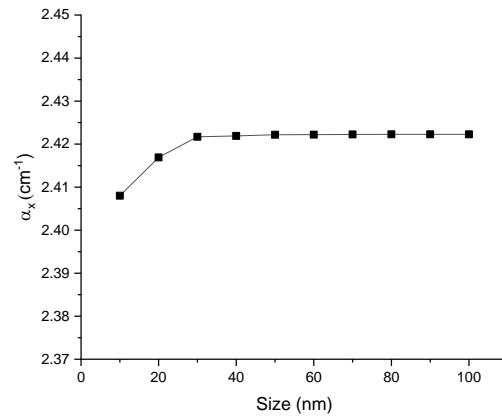


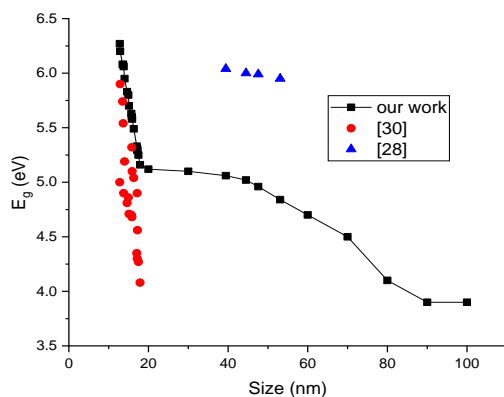
Fig. 8. The calculated x component of absorption coefficient ( $\alpha_x$ ) of simulated KTP spherical nanoparticles with different diameters.

Table 4. Simulation results for the components of absorption coefficient of KTP spherical nanoparticles with different sizes.

Size (nm)	$\alpha_x$	$\alpha_y$	$\alpha_z$
10	2.4080	5.0591	18.6176
20	2.4169	5.0853	18.7139
30	2.4217	5.0878	18.7203
40	2.4219	5.0886	18.7263
50	2.4221	5.0887	18.7273
60	2.4222	5.0892	18.7282
70	2.4222	5.0892	18.7283
80	2.4222	5.0893	18.7284
90	2.4222	5.0893	18.7285
100	2.4222	5.0893	18.7285

A blue-shift occurs in the wavelength of absorption edge at the nanoscale as a result of decreasing particle size [45, 46] and this is responsible for the increase of band gap energy [15, 47]. It has been reported that bulk KTP crystal exhibits an absorption edge at the wavelength of 350 nm and its band gap energy is in the range of 3.47 eV to 3.8 eV [5, 7, 11]. The band gap values of simulated KTP spherical nanoparticles are calculated based on equations (13) and (18), and the results are shown in Figure 9. Here, in order to investigate the effects of particle size on band gap energy and absorption edge wavelength, in addition to the

parametric solution for particles from 10 to 100 nm with a step of 10 nm, the experimentally reported results in the literature (ref [28,30]) for KTP nanoparticles with the particle sizes of 54, 53.08, 47.58, 44.5, 39.42, 17.89, 17.47, 17.24, 17.19, 17.16, 17.06, 16.31, 15.90, 15.86, 15.71, 15.11, 14.95, 14.61, 14, 13.76, 13.64, 13.49, 12.90, 12.78, and 12 nm are also simulated for more exact comparison with the experimental data. Figure 9 indicates the significant influence of KTP particle size on the band gap, specifically a dramatic decrease of band gap is observed when the particle size increases from 10 to 20 nm. However, further increase in particle size results in only slight decrements of band gap. Also, for the particle sizes of 20 to 40 nm, a saturation of band gap occurs at 5 eV. These results show that the band gap energy decreases with increasing particles size, and the band gap energy of nanoparticles is greatly higher than its corresponding bulk material. To further investigate the effects of nanoparticle size on band gap energy, the simulation results are compared with the experimental results from the literature. To compare the obtained results with the previously reported experimental results, nanoparticles with different sizes that reported in experimental data [28, 30], have been also considered for simulation. This comparison indicates that our simulation results and the experimental data especially for particles with a size of 13 to 18 nm, are well consistent with only ignorable differences. The observed difference between the simulation and experimental results in other data ranges can be expected and justified due to different synthesis methods and conditions used in experimental works [28, 30] and diverse assumptions and theories considered in the simulation with the finite element method.



**Fig. 9.** Simulated band gap energy of KTP nanoparticle as a function of particle size. Experimental data from references [28] and [30] are shown in the figure for comparison.

The photonic band gap of KTP nanoparticles was also investigated theoretically by COMSOL Multiphysics and Rsoft softwares. A photonic crystal can be simply defined as a medium with highly dispersive alternating optical properties, whose transmission and reflection strongly depend on the wavelength of radiation. The constant or grid periodicity of this structure,  $a$ , represents the minimum length of the space in which the grid structure is repeated. In a photonic crystal, the permittivity is defined as an alternating spatial function. Periodicity primarily creates continuous and borderless limits in the frequency domain, preventing wave propagation within the structure.

These regions are called the photonic band gap or frequency band. Between two consecutive photonic slits, there is an allowed frequency band (and vice versa) where wave propagation is possible under certain conditions. In photonic crystals, just like Bravais crystal groups in solid state physics, two-dimensional geometries can be divided into five main families. But only two crystal groups (square structure and triangular structure) are important in two dimensions. For reasons such as the complete and effective reflection of the photonic crystals and the zero density of states in the photonic gap, photonic crystals have a privileged position in optoelectronics. Most of the time, information about the band structure in one-, two-, or three-dimensional photonic crystals is only needed along the edges of the Brillouin zone [48-50].

The changes in the photonic gaps of KTP nanoparticles as a function of particle size simulated by COMSOL Multiphysics and Rsoft softwares are shown in Figures 10 and 11, respectively. Since the distance between particles in the photonic structure is assumed to be a multiple of the radiation wavelength; depending on the distance between the particles, the waves in the photonic gap are reflected instead of propagating in the structure. The vertical axis in Figures 10 and 11 represents dimensionless quantity of normalized frequency ( $a/\lambda$ ), and the horizontal axis represents  $k$ , where  $a$  is the distance between particles,  $\lambda$  is the radiation wavelength, and  $k$  is the wavenumber. The results obtained from COMSOL and Rsoft softwares confirm each other with a slight error, as can be observed in Figures 10 and 11. According to these Figures, the dimensionless quantity of photonic gap width decreased from 0.1 to 0 when particle size increased from 20 nm to 50 nm. Therefore, this effect becomes visible only for particle sizes below 30 nm.

In summary, the results indicate that the size of KTP particles can greatly regulate the optical characteristics of KTP crystals at the nanoscale. Their innovative and wide-ranging applications in optical devices and processes, such as nanofilter membranes, waveguides, second harmonic generation, and nanosensors, can stem from their dependence on particle size and the enhancement of optical properties with size [14, 26, 29].

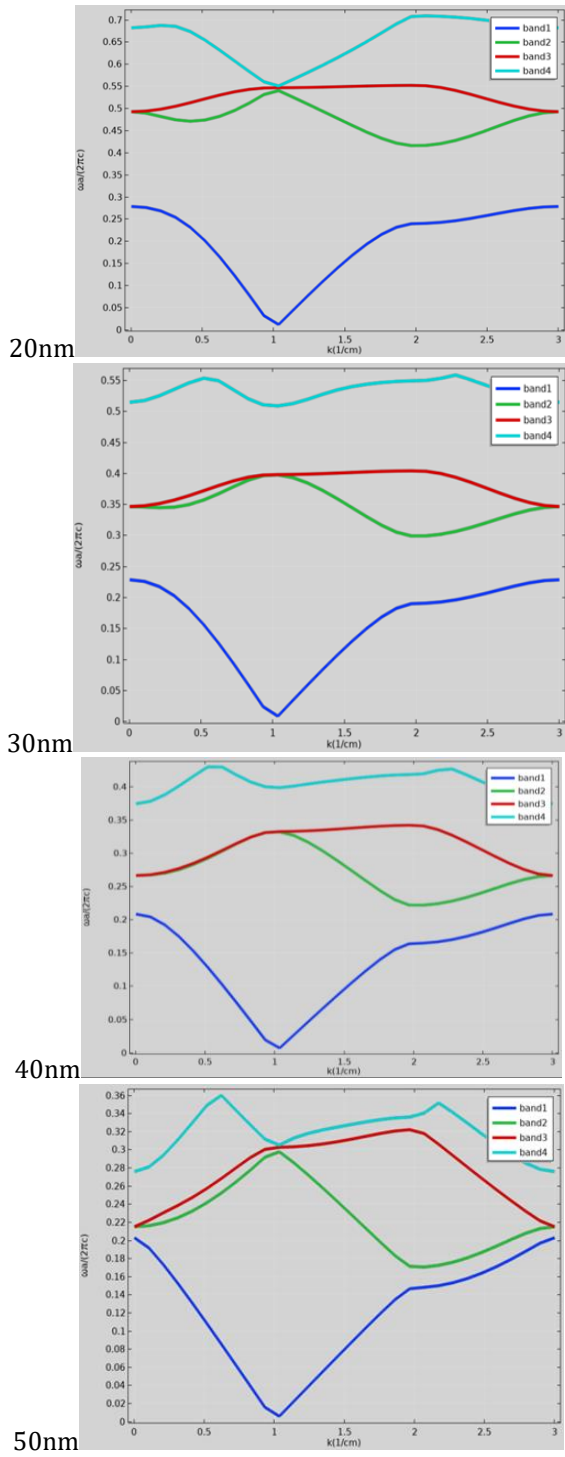


Fig. 10. Simulation results for photonic gap of KTP nanoparticles with different sizes obtained by COMSOL Multiphysics software.

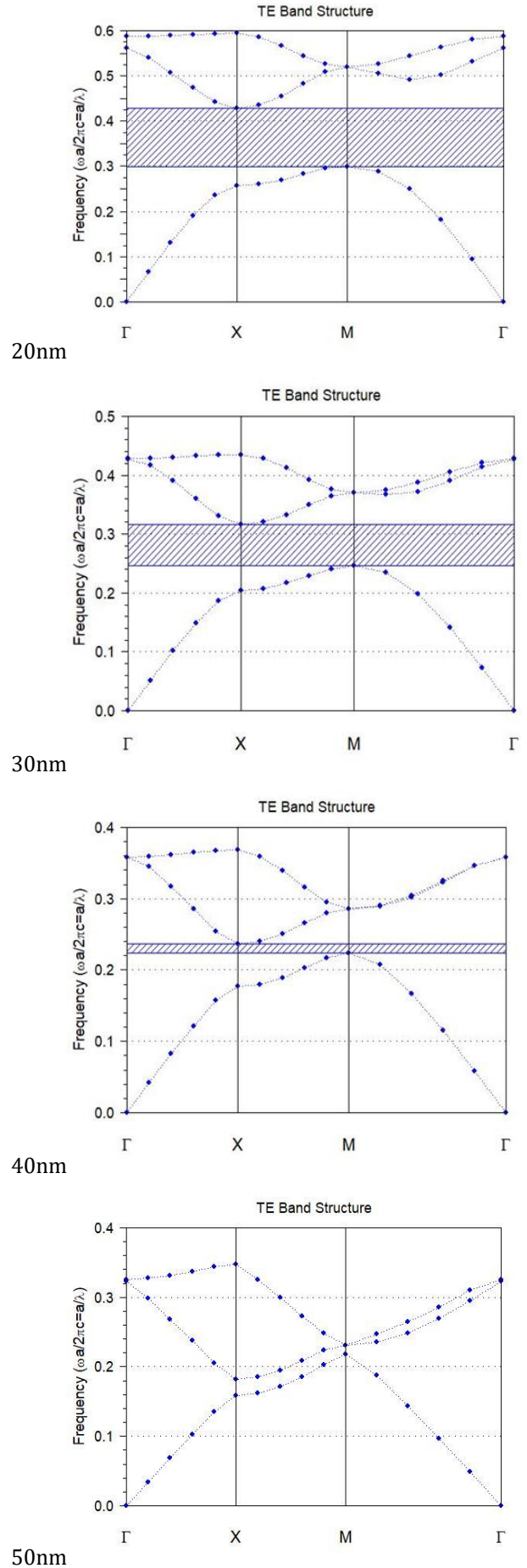


Fig. 11. Simulation results for photonic gap of KTP nanoparticles with different sizes obtained by Rsoft software.

#### 4. Conclusion

Using COMSOL Multiphysics software for computer simulation, the impact of particle size on the optical characteristics of spherical KTP nanoparticles was examined theoretically in this study. The results showed that reducing the size of KTP nanoparticles under irradiated light with a specific wavelength has different effects on the refractive index, cut-off wavelength, scattering cross section, band gap energy, and photonic gap. So that, by reducing the particle size, the refractive index, cut-off wavelength, and scattering cross section decreased, but the band gap energy increased to about 6.2 eV when the particles size decreased to 10 nm. Also, the dimensionless quantity of photonic gap width increased from 0 to 0.1 when particles size decreased from 50 nm to 20 nm. Also, increasing the wavelength of irradiated light from 400 nm to 1000 nm on a nanoparticle with a specific size gradually reduced its refractive index and scattering cross section. Thus, the obtained results show that the size of KTP nanoparticles is an important and influential factor on their optical properties, so reducing the size of nanoparticles, specifically below 30 nm, can significantly control their optical properties. These simulated results were also compared with available experimental data from the literature and discussed.

#### Acknowledgements

This research received no external funding.

#### Conflicts of Interest

The author declares that there is no conflict of interest regarding the publication of this article.

#### References

- [1] Li, S.-L., Y. Song, L.-N. Ma, and H.-L. Wang, 2024. Femtosecond-laser-inscribed cladding waveguides in KTiOPO<sub>4</sub> crystal for second-harmonic generation and Y-branch splitters. *Frontiers in Physics*, 12, pp. 1341210.
- [2] Zhou, H., X. He, W. Wu, J. Tong, J. Wang, Y. Zuo, Y. Wu, C. Zhang, and Z. Hu, 2023. Hydrothermal growth of KTiOPO<sub>4</sub> crystal for electro-optical application. *Light: Science & Applications*, 12(1), pp. 23.
- [3] Taziev, R. and V. Atuchin, 2022. Analysis of SAW Temperature Properties in KTiOPO<sub>4</sub> Single Crystal. *Materials*, 16(1), pp. 69.
- [4] Guretskii, S., I. Kolesova, A. Kravtsov, A. Mit'kovets, E. Trukhanova, and A. Linkevich, 2015. Effect of growth conditions on the optical homogeneity of KTiOPO<sub>4</sub> crystals. *Inorganic Materials*, 51, pp.913-915.
- [5] Zumsteg, F., J. Bierlein, and T. Gier, 1976. K x Rb1- x TiOPO<sub>4</sub>: a new nonlinear optical material. *Journal of Applied Physics*, 47(11), pp. 4980-4985.
- [6] Sadhasivam, S., R.N. Perumal, and P. Ramasamy, 2015. Flux growth and grey colouration characteristics in KTiOPO<sub>4</sub>: Ln (Ln= Yb, Nd, Ho, Er, La). *Journal of crystal growth*, 431, pp.32-38.
- [7] Bierlein, J.D. and H. Vanherzeele, 1989. Potassium titanyl phosphate: properties and new applications. *JOSA B*, 6(4), pp. 622-633.
- [8] Bordui, P.F. and M.M. Fejer, 1993. Inorganic crystals for nonlinear optical frequency conversion. *Annual Review of Materials Science*, 23(1), pp. 321-379.
- [9] Maslov, V.A., V. Mikhailov, O.P. Shaunin, and I.A. Shcherbakov, 1997. Nonlinear absorption in KTP crystals. *Quantum Electronics*, 27(4), pp. 356.
- [10] Mamrashev, A., N. Nikolaev, V. Antsygin, Y. Andreev, G. Lanski, and A. Meshalkin, 2018. Optical properties of KTP crystals and their potential for terahertz generation. *Crystals*, 8(8), pp. 310.
- [11] Kannan, C., S. Ganesamoorthy, A. Miyazaki, H. Kimura, and P. Ramasamy, 2005. Effect of chromium on optical and electrical properties of self-flux grown KTiOPO<sub>4</sub> single crystals. *Ferroelectrics*, 326(1), pp. 123-128.
- [12] Elaheh, G. and J.T. Majid, 2015. The effect of cooling rate on size, quality and morphology of KTiOPO<sub>4</sub> (KTP) crystals grown by different nucleation techniques. *Crystal Research and Technology*, 50(8), pp. 603-612.
- [13] Roth, M. and M. Tseitlin, 2010. Growth of large size high optical quality KTP-type crystals. *Journal of crystal growth*, 312(8), pp. 1059-1064.
- [14] Galceran, M., M. Pujol, J. Carvajal, S. Tkaczyk, I. Kityk, F. Díaz, and M. Aguiló, 2008. Synthesis and characterization of KTiOPO<sub>4</sub> nanocrystals and their PMMA nanocomposites. *Nanotechnology*, 20(3), pp. 035705.
- [15] Goyal, M. and M. Singh, 2020. Size and shape dependence of optical properties of nanostructures. *Applied Physics A*, 126, pp.1-8.
- [16] Jalava, J.-P., V.-M. Taavitsainen, R.-J. Lamminmäki, M. Lindholm, S. Auvinen, M. Alatalo, E. Vartiainen, and H. Haario, 2015. Modeling TiO<sub>2</sub>' s refractive index function from bulk to nanoparticles. *Journal of Quantitative Spectroscopy and Radiative Transfer*, 167, pp.105-118.
- [17] Patel, G. and T. Pandya, 2018. Effect of size and shape on static Refractive Index, Dielectric constant and Band gap of Nano solids. *Physics and Applied Sciences*, 6(1), pp. 37-42.
- [18] Arora, N. and D.P. Joshi, 2017. Thermodynamic study of nanometals for different shapes and sizes . *Indian J Pure & Appl Phys*, 55, pp. 284-292.
- [19] Baral, B., A. Altaee, K. Simeonidis, and A.K. Samal, 2024. Shape and size dependent nanostructures for environmental applications. *Frontiers in Chemistry*, 12, pp.1-5
- [20] Pachauri, U., D.P. Joshi, and N. Arora, 2020. Theoretical model for size, dimension and shape effect on electrical behavior of semiconductor nanomaterials. *Applied Physics A*, 126, pp.1-11.
- [21] Tohgha, U.N., J.T. Ly, K.M. Lee, Z.M. Marsh, A.M. Watson, T.A. Grusenmeyer, N.P. Godman, and M.E. McConney, 2024. Switchable Optical Properties of Dyes and Nanoparticles in Electrowetting Devices. *Nanomaterials*, 14(2), pp. 142.

- [22] Altammar, K.A., 2023. A review on nanoparticles: characteristics, synthesis, applications, and challenges. *Frontiers in Microbiology*, 14, pp.1155622.
- [23] Qi, W., 2005. Size effect on melting temperature of nanosolids. *Physica B: Condensed Matter*, 368(1-4), pp. 46-50.
- [24] Abbasi, R., G. Shineh, M. Mobaraki, S. Doughty, and L. Tayebi, 2023. Structural parameters of nanoparticles affecting their toxicity for biomedical applications: a review. *Journal of Nanoparticle Research*, 25(3), pp. 43.
- [25] Malekfar, R., A. Cheraghi, G. Ahmadi, and M. Khanzadeh, 2009. Raman Spectra and Structural Data of the Nanocrystalline KTP (KTiOPO<sub>4</sub>) Synthesized by Pechini Method. *Acta Physica Polonica A*, 116(6), pp. 1073-1075.
- [26] Malekfar, R., G. Ahmadi, A. Cheraghi, J. Rohollahnejad, F. Sahraiyani, and M. Khanzadeh, 2009. Micro-Raman scattering of KTP (KTiOPO<sub>4</sub>) nanocrystallites synthesized by modified sol-gel Pechini method. *Vibrational Spectroscopy*, 51(2), pp. 308-312.
- [27] Biswas, S.K., A. Pathak, and P. Pramanik, 2007. Synthesis of nanocrystalline ktiopo4 powder by chemical method. *Journal of the American Ceramic Society*, 90(4), pp. 1071-1076.
- [28] Gharibshahian, E., M.J. Tafershi, and M. Fazli, 2018. Effects of solution concentration and capping agents on the properties of potassium titanyl phosphate nanoparticles synthesized using a co-precipitation method. *Journal of Physics and Chemistry of Solids*, 116, pp.241-249.
- [29] Gharibshahian, E., M.J. Tafreshi, and M. Behzad, 2020. The effects of solution pH on structural, optical and electrical properties of KTiOPO<sub>4</sub> (KTP) nanoparticles synthesized by hydrothermal method. *Optical Materials*, 109, pp.110230.
- [30] Madari, N., E. Gharibshahian, and M. Tafreshi, 2022. Novel synthesis of KTP nanoparticles by combustion method using urea and glycine fuels. *Applied Physics A*, 128, pp.1-14.
- [31] Wnuk, P., L. Le Xuan, A. Slablab, C. Tard, S. Perruchas, T. Gacoin, J.-F. Roch, D. Chauvat, and C. Radzewicz, 2009. Coherent nonlinear emission from a single KTP nanoparticle with broadband femtosecond pulses. *Optics Express*, 17(6), pp. 4652-4658.
- [32] Nguyen, D.T.T. and N.D. Lai, 2019. Deterministic insertion of KTP nanoparticles into polymeric structures for efficient second-harmonic generation. *Crystals*, 9(7), pp. 365.
- [33] Zhou, C., L. Le Xuan, A. Slablab, N. Sandeau, S. Brasselet, D. Chauvat, and J.-F. Roch, 2008. Investigation of KTiOPO<sub>4</sub> nanocrystals by means of second-harmonic light emission. *Chinese Optics Letters*, 6(1), pp. 64-67.
- [34] Nikolaev, I.V. and N.G. Korobeishchikov, 2021. Influence of the Parameters of Cluster Ions on the Formation of Nanostructures on the KTP Surface. *Applied Nano*, 2(1), pp. 25-30.
- [35] Fan, X., W. Zheng, and D.J. Singh, 2014. Light scattering and surface plasmons on small spherical particles. *Light: Science & Applications*, 3(6), pp. e179-e179.
- [36] Mie, G., 1908. Beiträge zur Optik trüber Medien, speziell kolloidaler Metallösungen. *Annalen der Physik*, 330(3), pp. 377-445.
- [37] Horvath, H., 2009. Gustav Mie and the scattering and absorption of light by particles: Historic developments and basics. *Journal of Quantitative Spectroscopy and Radiative Transfer*, 110(11), pp. 787-799.
- [38] Gharibshahi, E., B.D. Young, A.S. Bhalla, and R. Guo, 2020. Theory, simulation and experiment of optical properties of cobalt ferrite (CoFe<sub>2</sub>O<sub>4</sub>) nanoparticles. *Journal of Materials Science & Technology*, 57, pp.180-187.
- [39] Gharibshahi, E. and M. Alamaniotis, 2022. Simulation and modeling of optical properties of U, Th, Pb, and Co nanoparticles of interest to nuclear security using finite element analysis. *Nanomaterials*, 12(10), pp. 1710.
- [40] Zutterman, F. and B. Champagne, 2021. Simulation of absorption and scattering spectra of crystalline organic nanoparticles with the discrete dipole approximation: Effects of crystal shape, crystal size, and refractive index of the medium. *The Journal of Chemical Physics*, 155(16), pp.164703.
- [41] Kato, K. and E. Takaoka, 2002. Sellmeier and thermo-optic dispersion formulas for KTP. *Applied optics*, 41(24), pp. 5040-5044.
- [42] Di Finizio, S., A. Peña, T. Trifonov, J. Carvajal, M. Aguiló, J. Pallarés, A. Rodriguez, R. Alcubilla, L. Marsal, and F. Díaz, 2006. Growth of 2D KTP photonic crystals for efficient second order nonlinear optical processes. in Photonic Crystal Materials and Devices III (ie V). *SPIE*, 6182, pp. 61820x1-61820x7.
- [43] Butt, H., T.D. Wilkinson, and G.A. Amaratunga, 2012. Fem modeling of periodic arrays of multiwalled carbon nanotubes. *Progress In Electromagnetics Research M*, 22, pp.1-12.
- [44] Makwana, M.P., R. Craster, and S. Guenneau, 2019. Novel topological beam-splitting in photonic crystals. *arXiv preprint arXiv Physics. Optics*, 2, pp.1902.00072.
- [45] Bora, T., A. Dousse, K. Sharma, K. Sarma, A. Baev, G.L. Hornyak, and G. Dasgupta, 2018. Modeling nanomaterial physical properties: theory and simulation. *International Journal of Smart and Nano Materials*, 1947-5411, pp. 1-28.
- [46] Anttu, N., H. Mäntynen, A. Sorokina, J. Turunen, T. Sadi, and H. Lipsanen, 2021. Applied electromagnetic optics simulations for nanophotonics. *Journal of Applied Physics*, 129(13), pp.131102.
- [47] Onyia, A.I., H.I. Ikeri, and A.I. Chima, 2020. Surface and quantum effects in nanosized semiconductor. *American Journal of Nano Research and Applications*, 8(3), pp. 35-41.
- [48] Yao, L., G. Huang, H. Chen, and M.V. Barnhart, 2019. A modified smoothed finite element method (M-SFEM) for analyzing the band gap in phononic crystals. *Acta Mechanica*, 230, pp.2279-2293.
- [49] Lucklum, F. and M.J. Vellekoop, 2018. Bandgap engineering of three-dimensional phononic crystals

in a simple cubic lattice. *Applied Physics Letters*, 113(20), pp.201902.

[50] Chang, Z., *Fundamentals of attosecond optics*. 2016: CRC press, chap1, pp.1-46.